



## Heterogeneous Forward and Backward Scattering Modulation by Polymer-Infused Plasmonic Nanohole Arrays

Journal:	<i>Journal of Materials Chemistry C</i>
Manuscript ID	TC-ART-01-2019-000070.R1
Article Type:	Paper
Date Submitted by the Author:	07-Feb-2019
Complete List of Authors:	Zhang, Shuaidi; Georgia Institute of Technology College of Engineering Yu, Shengtao; Georgia Institute of Technology, Materials Science and Engineering Zhou, Jing; Georgia Institute of Technology College of Engineering, Materials Science and Engineering Ponder, James; Georgia Institute of Technology Smith, Marcus J.; Georgia Institute of Technology Reynolds, John; Georgia Institute of Technology, Chemistry and Biochemistry, Materials Science and Engineering Tsukruk, Vladimir; Georgia Institute of Technology, School of Materials Science and Engineering

## Heterogeneous Forward and Backward Scattering Modulation by Polymer-Infused Plasmonic Nanohole Arrays

*Shuaidi Zhang<sup>†</sup>, Shentao Yu<sup>†</sup>, Jing Zhou<sup>†</sup>, James F. Ponder Jr.<sup>‡§</sup>, Marcus J. Smith<sup>†#</sup>,  
John R. Reynolds<sup>‡</sup>, Vladimir V. Tsukruk<sup>\*†</sup>*

<sup>†</sup> School of Materials Science and Engineering, Georgia Institute of Technology, Atlanta, Georgia 30332, United States

<sup>‡</sup> School of Chemistry and Biochemistry, School of Materials Science and Engineering, Center for Organic Photonics and Electronics, Georgia Tech Polymer Network, Georgia Institute of Technology, Atlanta, Georgia 30332, United States

<sup>§</sup> Department of Chemistry, Imperial College London, London, W7 2AZ, United Kingdom

<sup>#</sup> Aerospace Systems Directorate, Air Force Research Laboratory, Wright-Patterson Air Force Base, Dayton, Ohio 45433, United States

### Abstract

The transmission and forward scattering of plasmonic nanohole arrays (NHAs) are widely examined in pursuit of non-fading plasmonic color filters for advanced displays and sensors. It is generally assumed that the reflection scattering is complementary to the corresponding transmission scattering and follows the same trend upon modulation of the dielectric environment. However, under oblique illumination, we observed peculiar and drastically different forward and backward scattering behavior of polymer-infused NHAs when a surrounding electrochromic polymer matrix was subjected to electrical potential, thereby changing the permittivity of the environment. Forward scattering at normal incidence angle of the NHAs is dominated by the extinction of the polymer coating, showing absorption-controlled attenuation behavior. In contrast, the concurrently monitored backward scattering at a highly oblique angle showed significant red-shifting in addition to attenuation. Our simulations suggest that the high incidence angle illumination in the backward scattering setup excites polarization dependent complex plasmon resonances that are highly sensitive to the modulation of the refractive index of the surrounding media. Such drastically different behavior of forward and backward scattering opens up possibilities for exploration of NHAs as prospective tunable reflection filters and colorimetric electrochemical sensors.

**Keywords:** Plasmonic metasurface, electrochromic polymer, tunable plasmonic response, nanohole array, sub-wavelength apertures

\* Corresponding author: vladimir@mse.gatech.edu

## Introduction

Controlled light transmission through sub-wavelength orifices in thin metallic films has been well documented.<sup>1, 2, 3</sup> This intriguing phenomenon is due to the excitation of a special kind of light coupled electron resonances at the metal-dielectric interface known as surface plasmonic polaritons (SPP).<sup>4</sup> By arranging plasmonic nanoholes of varying dimensions into large arrays of different periodicity and symmetry, different plasmon resonances can be excited by incident light, thus different light transmission properties can be achieved.<sup>5, 6</sup> Several pioneering papers have already examined in detail the theoretical aspects of such optical element.<sup>7</sup> Some even explored more advanced geometries such as aligned multilayered nanohole array (NHA), where the intercoupling between SPPs at different interfaces can modulate the transmission peak or even lead to new resonant modes;<sup>8</sup> or air gap coupled NHA, where the width of the air gap can be used to induce constructive or destructive interference.<sup>9</sup>

Because transmission spectra can be modified by changing the nanohole array geometry, there has been great interest to utilize them as pre-programmed color filters for advanced imaging and display technologies.<sup>10, 11, 12, 13, 14</sup> Multiple studies have been conducted on the use of diverse NHAs coupled with nematic liquid crystals, electrochromic polymers, and Fabry–Pérot devices as plasmonic filters that can be turned on and off by electrical signals.<sup>15, 16, 17, 18, 19</sup> Recent explorations in novel NHA structures, such as asymmetric nanoholes, demonstrated polarization dependent colors.<sup>20</sup> Fabricated metal-insulator-metal multilayered nanoholes have demonstrated the ability to support Fano resonances with enhanced sensitivity to refractive index changes of the surrounding media.<sup>21</sup>

However, while these studies focused on the forward scattering properties of NHAs, which are immediately relevant to backlit color displays, little attention has been paid to their backward scattering properties, especially when illuminated at oblique angles. In fact, there is a good reason to expect the optical response of periodic plasmonic nanoarrays to be drastically different when they are used as backward scatterers, since it is already known that the transmission profiles of plasmonic NHAs are angle dependent.<sup>22</sup> However, monitoring of both forward and backward scattering under variable refractive conditions is rarely conducted due to experimental challenges.

In this study, we investigate both the forward and backward scattering of NHAs infused with a redox active electrochromic polymer (ECP), poly(2,2'-bis(2-ethyl-hexyloxymethyl)-3,4-propylenedioxythiophene) (ECP-M), which switches between a purple/magenta neutral state and a highly transmissive oxidized state, with modulated refractive index (Figure 1). The modulation of the dielectric environment is accomplished conveniently and reversibly via applied electrochemical potential in an electrolyte.<sup>23, 24, 25, 26</sup> It was found that there are indeed significant differences in backward and forward scattering characteristics, especially in their relative sensitivity to refractive index modulations. When subjected to an applied potential, spectra measured in the forward scattering mode shows selective attenuation, while spectra measured in the backward scattering mode shows single-peak red-shifting. Electrodynamic simulations show that these differences are due to the highly oblique illumination used for backward scattering, exciting multiple complex plasmon resonances that collectively influence the integrated optical output.

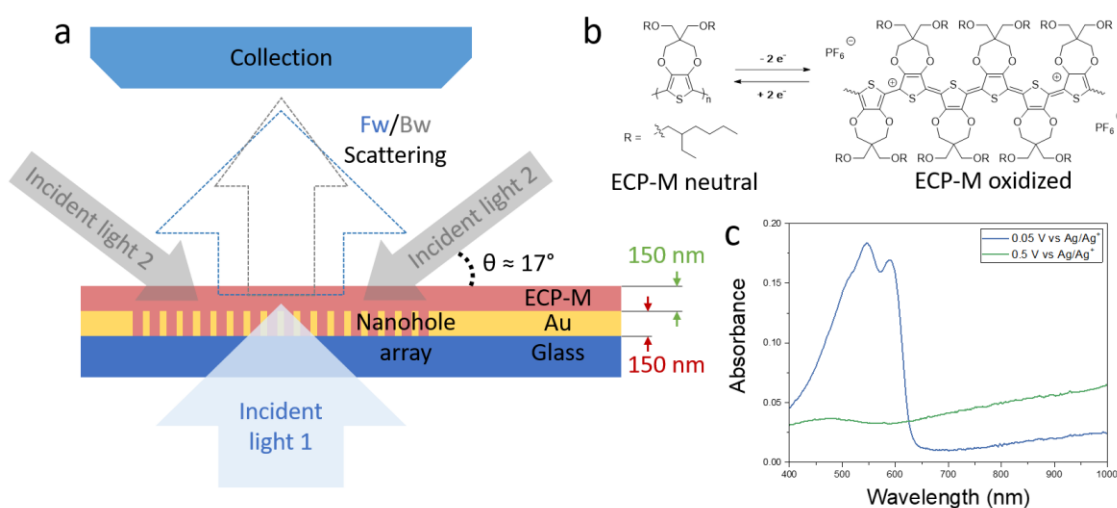


**Figure 1.** (a) The experimental setup of ECP-M infused Au NHA on glass slides. In forward scattering measurement, light comes in from the bottom (incident light 1) and is collected at the top (blue dashed arrow). In backward scattering measurement, light comes from the top at 73° incidence angle (incident light 2) and is collected at the top (grey dashed arrow). (b) Molecular structure and electrochemical switching of ECP-M. (c) UV-vis spectra of ECP-M in neutral (blue) and oxidized (green) states.

## Experimental

### Materials

Tetrabutylammonium hexafluorophosphate (TBAPF<sub>6</sub>) and propylene carbonate (PC) were purchased from Sigma Aldrich and used without further purification. The ECP-M electrochromic polymer was synthesized as described previously from the corresponding alkoxy-substituted 3,4-propylenedioxythiophene monomer by oxidative polymerization with iron(III)chloride.<sup>26</sup> The molecular mass of the polymer is 12.4 kDa with a dispersity ( $\bar{D}$ ) of 1.8 as determined by gel permeation chromatography (GPC) in tetrahydrofuran (THF) versus polystyrene (PS) standards.<sup>30</sup>

### ***Fabrication of NHA***

The plasmonic NHA was manufactured via focused ion beam (FIB) direct writing lithography. First, 150 nm thick of Au film is evaporated onto glass slides using Denton Explorer E-beam evaporator at a rate of 0.5 Å/s at 10<sup>-6</sup> Torr. The deposition is monitored by a quartz microbalance mass sensor. Next, the substrate is transferred to the FEI Nova Nanolab 200 FIB/SEM system for patterning. Specific nanohole patterns were etched by Ga<sup>+</sup> ion beam operated at 30 kV 10pA following corresponding bitmap files. After initial optical characterization of the pristine nanoholes. 20 μL of concentrated ECP-M toluene solution was spincoated onto the NHA substrate at 2000 rpm, resulting in a 150-nm thick film.

### ***Electrochemical switching***

Electrochemical measurements were carried out using a VersaSTAT3-200 (Princeton Applied Research) with Versastudio software in a three-electrode cell with a Ag/Ag<sup>+</sup> reference electrode (10 mM AgNO<sub>3</sub> in 0.5 M TBAPF<sub>6</sub>/ACN,  $E_{1/2}$  is 76 mV for ferrocene), a Pt wire as the counter electrode, and Au coated substrate with patterned NHAs as the working electrode.<sup>34</sup> The electrolyte is 0.5 M TBAPF<sub>6</sub> in PC, individual switching is done using chronoamperometry setting holding the working electrode at designated potential against reference electrode for 10 s. Cycling experiment was performed using cyclovoltammetry setting at scan speed of 0.2 V/s.

### ***Optical characterization***

The extinction spectra of NHAs and spectral mapping were acquired by CytoViva hyperspectral scanning system with a SPECIM Inspector V10E spectrograph (30μm slit width, spectral range: 400–1000 nm, dispersion: 97.5 nm/mm, spectral resolution: 2.8 nm) coupled with a PCO.pixelfly camera using a 50x (NA = 0.8) objective which has a fixed ~73° incidence cone when used in dark field mode. A Fiber-Lite DC-950 halogen lamp is used as the light source. The Lamp spectrum is collect in the transmission setup without any substrate. All the spectra were collected at max output of the lamp and normalized by dividing the lamp spectrum. All measurements done in air, the oxidative state of the substrate is switched in an electrochemical cell between measurements in electrolyte and systems were completely dried before optical measurements.

UV-vis extinction spectra were collected using a Shimadzu UV-vis-2450 spectrometer with D2 and tungsten lamps (wavelength range: 300–1100 nm). The extinction spectra

of ECP-M are collected using 150 nm pure ECP-M film on ITO substrate with extinction from the blank ITO subtracted. The substrate is then placed into the electrochemical cell, switched to another oxidation state, dried, and measured again.

### ***FDTD simulations***

FDTD simulations were conducted using Lumerical FDTD Solutions (Version 8.19).<sup>27</sup> An array of 9 nanoholes (3 holes each in two primary axis) of specified periodicity, diameter and symmetry were modeled as through holes in a 150-nm thick Au film on top of 1-micron thick SiO<sub>2</sub> and filled with respective dielectric materials (air, ECP-ox, ECP-neu). An additional 150-nm thick ECP film of respective oxidative states is constructed on top of the Au film when simulating ECP coated NHAs. The refractive index values of SiO<sub>2</sub> and gold were taken from previous reports or CRC Handbook.<sup>28,29</sup> The refractive index values of ECP-M at oxidized and neutral states were taken from previous work where they were measured for thin films with spectroscopic ellipsometry.<sup>30</sup>

The simulation region was restricted to the center unit cell defined in the x,y Cartesian coordinates with 1 micron z span. A mesh override was applied to the nanoholes with a 10 nm mesh size and 10 nm buffer in the x-, y-, and z-directions. For simulation of forward scattering, a broadband Bloch planewave source with 400-1000 nm wavelength span was used for illumination. The injection plane was placed inside the SiO<sub>2</sub> substrate with propagation direction pointing upward at normal incidence angle. Periodic boundary conditions were applied in both x and y directions. Anti-symmetric and symmetric symmetries are applied to reduce simulation time. 12-layer perfect matched layer (PML) boundary condition was applied in the z direction to absorb radiation energy with minimum scattering. For simulation of backward scattering, a narrowband (band width: 8.825 THz) Bloch planewave source defined in the time domain with 50 fs pulse length and 100 fs offset is used for illumination. The injection plane was placed above the structures in air with propagation direction pointing downward at 73° incidence angle. Bloch boundary conditions were applied in both x and y directions. Anti-symmetric symmetry was applied to reduce simulation time. 36-layer PML boundary condition was applied in the z direction to absorb radiation energy with minimum scattering. The source frequency was swept from 300 THz to 750 THz in 200 individual simulations data at center frequency was recorded and compiled to yield a full spectrum.

## **Results and discussion**

### ***NHA, ECP-M, and illumination setup***

NHAs with different diameter, periodicity, and symmetry are fabricated on 150 nm thick E-beam evaporated Au on glass substrates using focused ion beam milling. Four different arrays were fabricated: p250s, p350s, p340h, and p420h. The arrays were identified by

their periodicity and symmetry as demonstrated in Figure 2a and Table 1. For example, p250s is a square (s) array with 250 nm periodicity, while p420h is a hexagonal (h) array with 420 nm periodicity. These geometric parameters of the NHAs are arbitrarily chosen based on previous research to test the universality of the ECP tuning effect.<sup>10</sup>

Table 1. Geometries of NHAs

NHA Designation	Periodicity (P)	Diameter (D)	Symmetry
p250s	$P_x=P_y=250$ nm	125 nm	Square
p350s	$P_x=P_y=350$ nm	175 nm	Square
p340h	340 nm	180 nm	Hexagonal
p420h	420 nm	240 nm	Hexagonal

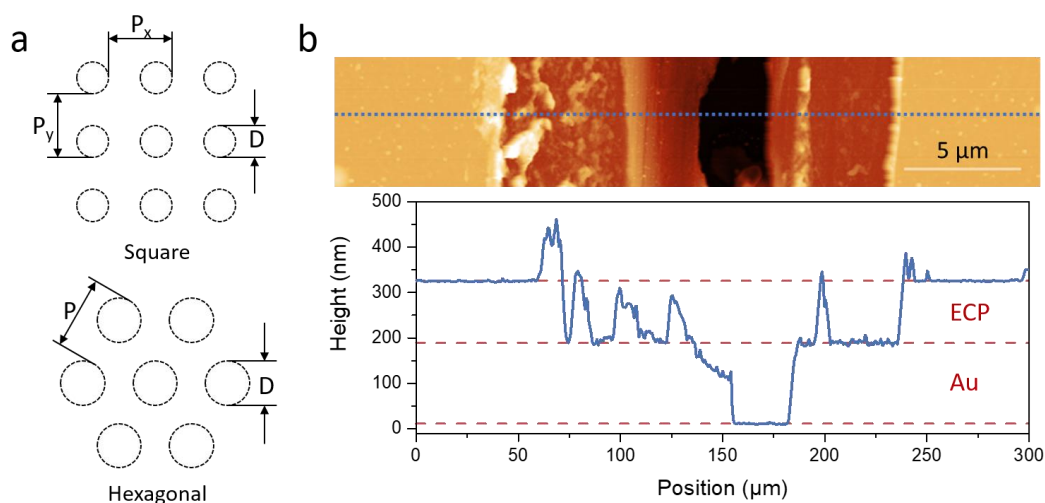


**Figure 2.** (a) The geometries and dimensions of the nanohole arrays. (b) AFM image of scratched ECP-Au-Glass structure, (Z scale: 500 nm) and cross-section profile along the dotted line, clearly showing the 3-layer structure.

After initial hyperspectral characterization of the as-fabricated NHAs, the entire substrate was coated with an additional  $\sim 150$  nm ECP film. Figure 2b shows the AFM image and the corresponding cross-sectional profile of a scratched line test on the pristine area of the substrate. A wide strip of ECP film cleanly separated at the ECP-Au interface upon incision and drag of the blade and reveals the Au film underneath. In the middle of the scratch line, where the tip of the blade sits, a narrow strip of Au is also scratched away, revealing the glass base.

Two illumination schemes are used to study the directional optical response of the ECP-M coated NHAs with all measurements conducted in air after film drying (Figure 1, see Experimental). In the forward scattering setup, broadband light from a halogen lamp illuminates the NHA at zero incidence through a glass substrate from beneath (Figure 1a, solid blue arrow). This essentially corresponds to the brightfield transmission mode in microscopy. The light is transmitted/forward scattered by the NHA and collected from above by an objective (Figure 1a, open blue arrow). In the backward scattering setup, light from the same source is introduced to the NHA at  $\sim 73^\circ$  (fixed by dark field objective) incidence through air from above (two solid gray arrows), scattered by the NHA, and collected by the same objective from above (Figure 1a, open gray arrow). This corresponds to the darkfield reflection mode in microscopy

Figure 3 shows the SEM and corresponding hyperspectral images of the as-fabricated NHAs (without ECP coating) at the two illumination conditions described above. Upon illumination, NHAs of different structural geometries display different colors, a clear indication of plasmonic effects. As the illumination condition changes, the observed color also changes correspondingly for each NHA. The colors are fairly consistent within each NHA. However, brightness non-uniformities and small color variations are present. These are mainly caused by defects and inhomogeneities during FIB milling. Unlike other finely grained metals like Al, E-beam evaporated Au films have grain size on the order of  $\sim 30$  nm (Figure S1a), ion milling of structures on a similar scale will inevitably yield less well-defined structures as the sputtering rate depends on the crystallographic orientation of the grain. As shown in Figure 3a, this nonuniformity in milling efficiency directly translates to some limited areas having blind holes instead of through holes, especially for arrays with smallest periodicity. Since plasmon resonances are dictated by structure geometry, such nonuniformity leads to the observed color/brightness differences. The effect is mitigated with larger hole diameter, causing p420h to have the highest brightness/color uniformity (Figure 3b, c).

In the backward scattering setup, we see another effect of imperfect FIB milling, the NHAs are surrounded by bright edges. This is due to the fact that despite the primary ion beam being blanked, the “un-milled” areas inside the arrays will still be partially etched from

secondary sputtering, resulting in NHAs having lower elevations than the rest of the Au film (Figure S1b-c). The elevation difference creates a step at the edge, which specularly reflects the oblique illumination into the collection objective. In addition, point like particulate contamination on Au surface can also be seen (Figure 3c). However, these contaminants do not appear to interfere with the NHA structures. These defects can all be eliminated by using single crystalline gold substrates in clean packaged environment, or by switching to other non-sticking, small grained plasmonic metals such as aluminum, should practical needs arise.

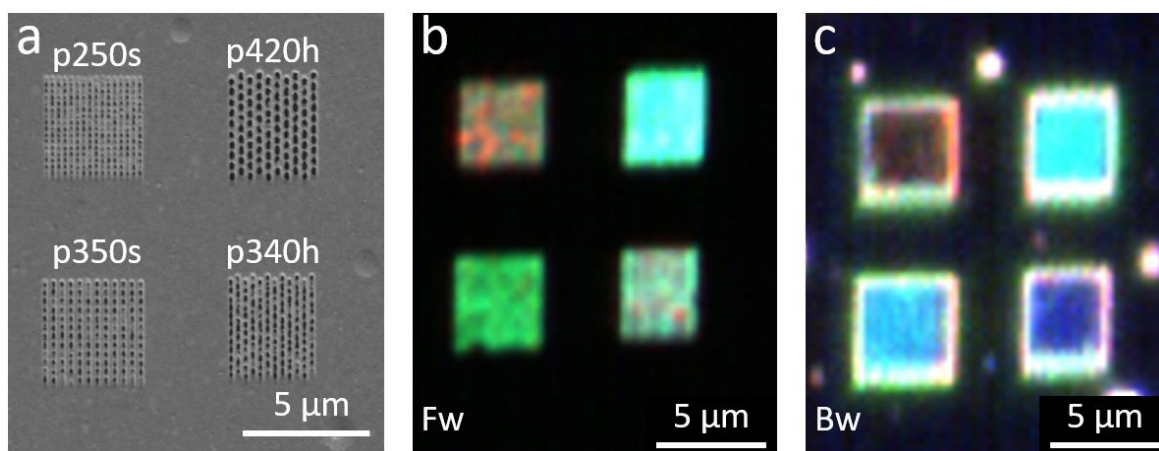


**Figure 3.** SEM image of NHAs with different geometries (see Scheme S1) (a). Hyperspectral image of the corresponding pristine arrays under forward (b) and backward (c) scattering illumination conditions.

The electron-rich alkoxy-substituted ECP-M was chosen as the electrochemically-controlled medium due to its excellent solvent compatibility, electrochemical stability, and low oxidation potential as was demonstrated earlier (see chemical structures in Figure 1b).<sup>30</sup> The polymer appears magenta/purple in its charge neutral state and, therefore, is termed ECP-Magenta (ECP-M).<sup>30</sup> ECP-M can be switched between neutral and oxidized states by applying an electrochemical potential at 0.05 V and 0.5 V vs. Ag/Ag<sup>+</sup>, respectively (Figure S2). In the neutral state, ECP-M has a broad absorption band from 410–620 nm with two absorption peaks at 547 nm and 588 nm (Figure 1c). Upon removal of electrons from the conjugated backbone, ECP-M transitions into a colorless and transmissive oxidized state at 0.5 V (Figure 1c). A low residual absorption remains across

the visible spectrum, resulting in near-complete visual transparency under these conditions (Figure 1c).

### **Electrochemical switching of ECP-M infused NHA**

Figure 4 shows the hyperspectral spectra and corresponding image from two different NHAs with the smallest (p250s) and the largest (p420h) hole diameters collected at two

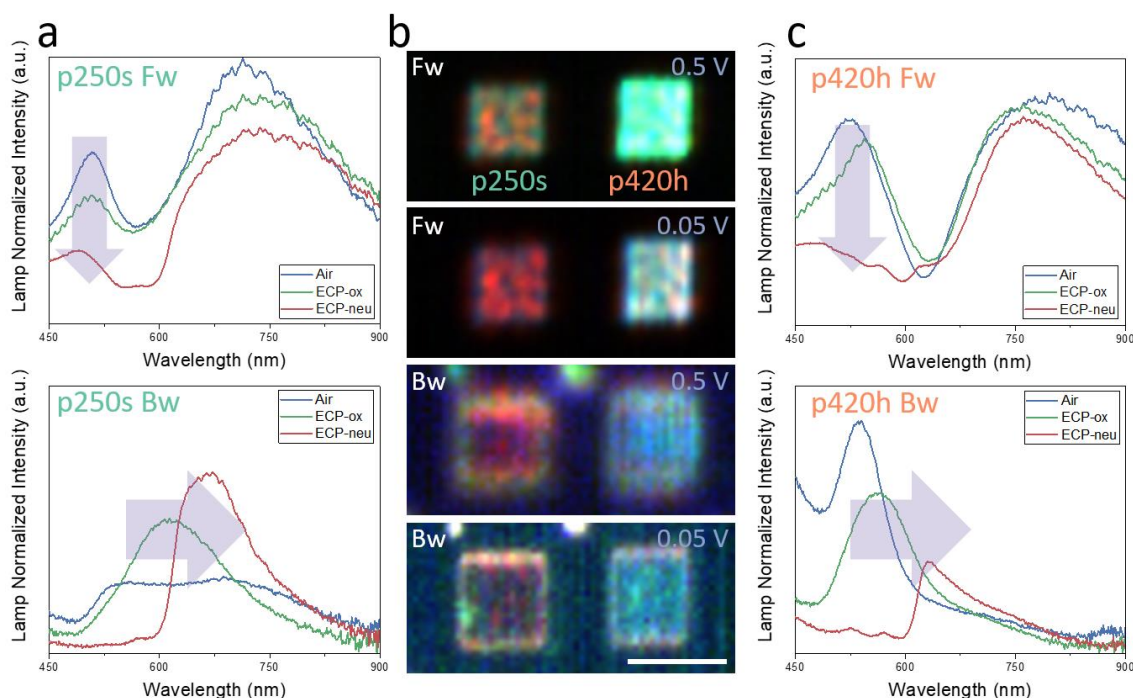


**Figure 4.** (a) Forward (Fw) and backward (Bw) scattering spectra of the p250s array in different dielectric environments: air, ECP-M in oxidized state (ECP-ox), and ECP-M in reduced state (ECP-neu). (b) Color image of p250s and p420h arrays under different ECP oxidation states: 0.5V (oxidized), 0.05 V (reduced). Scale bar: 5 μm. (c) Fw and Bw scattering spectra of the p420h array in different dielectric environments.

different illumination conditions and different dielectric environments: bare nanoholes and nanoholes covered by ECP coating in the oxidized state (ECP-ox) and in the neutral state (ECP-neu). Before coating with the ECP, the forward scattering spectrum of p250s NHA shows two broad plasmon resonances at ~510 nm and ~720 nm due to the excitation of surface plasmon resonances at the metal/air and at the metal/glass interface, respectively (Figure 4a).<sup>11</sup> ECP-M in its oxidized state does not affect these two peaks besides overall modest intensity damping due to non-specific light absorption (Figure 4a). The lack of modulation is also evident from the absence of color change between the forward scattering images of the respective array in Figure 3b and Figure 4b.

In contrast, when the ECP-M coating is switched to the neutral state by applying an electrical potential of 0.05 V, the plasmon peak at ~510 nm became severely attenuated while the peak at ~720 nm remained largely unaffected (Figure 4a). The selective damping of the ~510 nm peak occurs because the presence of ECP-M's absorption band is in this wavelength range (Figure 1c). Such selective damping causes the substantial changes in the color of the NHA, changing it from brown to red (Figure 4b)

When the illumination conditions are switched to those in backward scattering measurements (Figure 1a, incident light 2), completely different optical responses are observed (Figure 4a). Backward scattering showed a single plasmon peak with sequential redshift from initial 548 nm for bare NHA to ~611 nm for ECP-oxidized state, and further to ~664 nm for ECP-neutral state (Figure 4a). The oxidized/neutral state switching of the ECP media also resulted in significant visual color change (from red to brown color, Figure 4b bottom two figures).

The same trends are even more pronounced in the optical responses of the p420h array with larger spacing and hole diameter of 240 nm (Figure 4c). In the forward scattering spectrum, we again see damping in the 450-600 nm range caused by increasing light absorption by the ECP coating. The intensity ratio between the two plasmon peaks at ~530 nm and ~765 nm changed about twofold, from 0.85 in the oxidized state to 0.40 in the neutral state. In the backward scattering, a single peak also sequentially redshifted to ~561 nm and ~633 nm after covering with ECP-ox and ECP-neu coatings (Figure 4c).

Figure 5 shows the forwarding and backward scattering spectra of all 4 NHAs of different periodicities, hole diameters and symmetries. All of them showed similar behavior, mainly peak attenuation in the 450-600 nm range for forward scattering (arrows in Figure 5a-d), and peak attenuation plus significant red-shifting in backward scattering (arrows in Figure 5e-h), suggesting such trends are a general property of polymer-infused NHAs and not restricted to a specific array configuration.

It is known that, because plasmon polaritons exist at metal surfaces, the mode frequency in any plasmonic system will necessarily depend on its dielectric environment.<sup>31</sup> As shown in our previous work with plasmonic nanostructures embedded in ECP coatings, this property can be exploited to electrically tune the wavelength of the extinction plasmonic

peaks of nanoparticles.<sup>30, 32, 33, 34</sup> By changing the refractive index of the medium the plasmonic nanoparticles are dispersed in, their localized surface plasmonic resonance (LSPR) peak can be shifted to higher or lower wavelengths depending on the changes in refractive index in the spectral region of interest and the geometry of the nanoparticle.<sup>35</sup> For instance, previous results employing Au nanorods coated by ECP-M shells showed plasmonic peak shifts of up to 30 nm.<sup>30</sup>

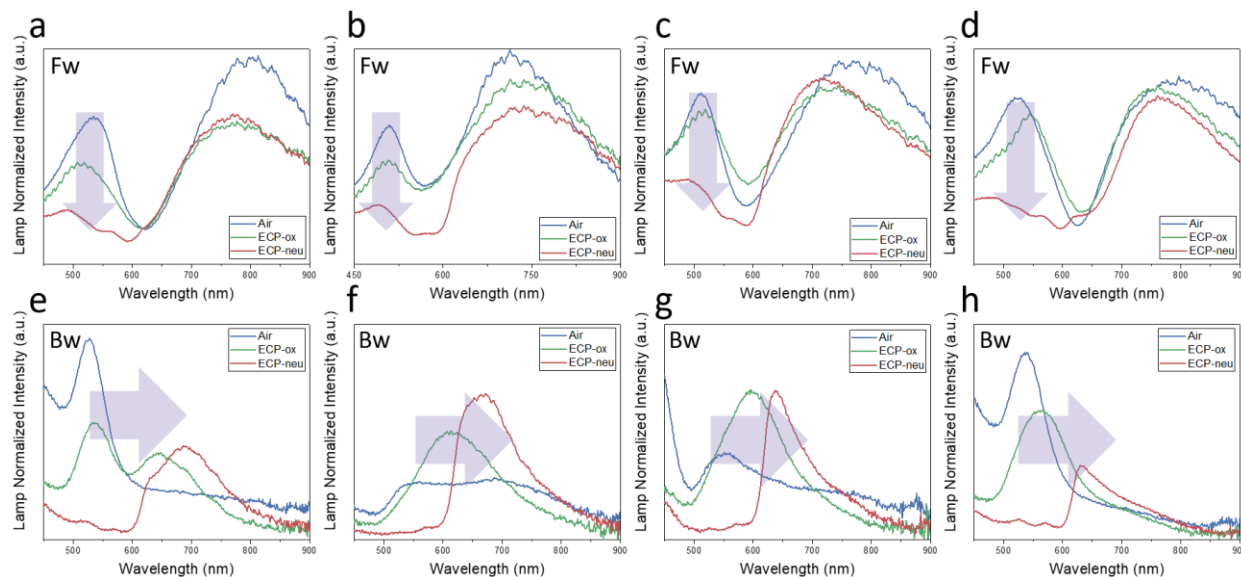


**Figure 5.** Forward scattering spectra of (a) p350s, (b) p250s, (c) p340h, (d) p420h arrays in air (blue), ECPox (green), and ECPrd (red). Backward scattering spectra of (e) p350s, (f) p250s, (g) p340h, (h) p420h arrays in air (blue), ECPox (green), and ECPrd (red).

Considering the present results, the NHA's response to changes in the dielectric environment is unexpected and cannot be explained by simple unidirectional radiation model that applies well to the individual randomly-oriented nanoparticles. In contrast, the spectral responses of the uniformly ordered NHAs are found to be highly dependent on the illumination conditions. For forward scattering, the lack of peak shifts means the plasmon resonance modes excited have low sensitivity towards the refractive index change, instead, the spectral changes are mainly produced by the attenuation by the ECP-M absorption. Yet, for backward scattering, the same ECP modulation produced very large red-shifts of the plasmon peak (70-120 nm), suggesting the plasmon modes excited in this illumination configuration are extremely sensitive to refractive index modulation.

For reference, we also calculated the color coordinates from the normalized spectrum of all the ECP infused NHAs in CIE 1931 color space (Figure S3). As expected, when ECP is switched from oxidized form to neutral form, the color coordinates shifted correspondingly. It is interesting to note that the shifts in color space are much larger in the backward scattering configuration as large spectral shifts are induced in addition to total intensity attenuation. The color range presented here are somewhat limited as we are primarily focused on the optical response of NHA under oblique illumination. For a wide range color palettes from plasmonic structures see several excellent examples.<sup>14, 36, 37, 38</sup>

### Theoretical aspects

To better understand the possible electrodynamics behind such behaviors, we further performed finite difference time domain (FDTD) simulations on the representative p250s NHA array. The simulation of forward scattering is straightforward, as light is injected and collected at the normal angle (Figure 6).<sup>39, 40</sup>

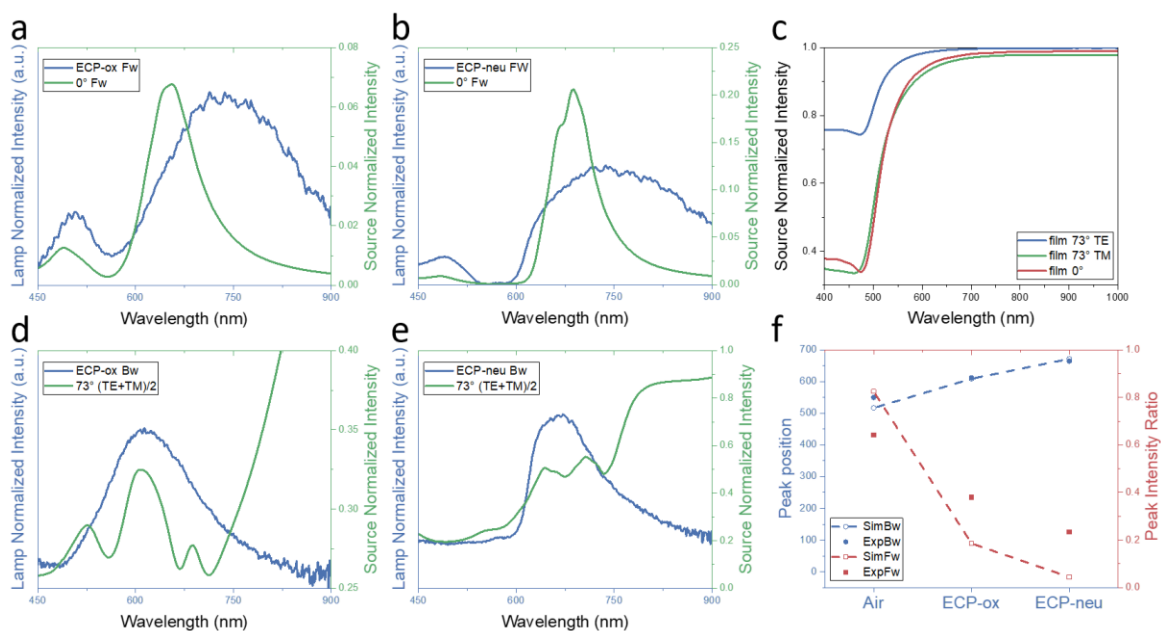


**Figure 6.** Measured forward scattering spectra (blue) of p250s array compared with FDTD results (green) for ECP oxidized (a) and reduced (b) states. (c) FDTD backward scattering results of 150 nm thick Au film at different angles and polarizations. Measured backward scattering spectra (blue) of p250s array compared with FDTD results (green) for ECP oxidized (d) and reduced (e) states. (f) Trends in experimental data and FDTD simulations in terms of peak intensity ratio for forward scattering and in terms of peak position for backward scattering.

Because the angle of incidence is  $0^\circ$ , there will be no phase difference on the incident light both spatially and temporally. In comparison, simulation of backward scattering is significantly more complex due to both interference from specular reflection and the phase difference build up among the frequency components at high incidence angle (see Figure S4 and relevant discussion in SI).

Furthermore, Figure 6 a, b shows the comparison between the FDTD simulations and measured results of the forward scattering of NHAs at different ECP oxidation states. As we can see from this comparison, the general spectral features, such as the existence of two plasmonic peaks and their relative intensities are well reproduced by FDTD. The simulation clearly showed the attenuation in the 450-600 nm range as the ECP coating is switched from ECP-ox to ECP-neu state. However, there is a blue-shift in the peaks and the measured spectra are broader than those simulated. These differences can be mainly attributed to defects in the NHAs with the holes being slightly larger than specified, causing a red shift from the ideal structures. In addition, the relatively large grain sizes of the evaporated Au film and resulting variations in hole dimensions broaden the plasmonic peak (Figure 3a).

On the other hand, in backwards scattering simulation, due to the periodic nature of the setup, light from specular reflection is included in simulated spectra (see discussion in SI). Thus, the spectra simulated all bear the hallmark, such as skewed high intensity in the infrared, of the reflection spectrum of bulk Au (Figure 6c red curve). In addition, because TE and TM polarized modes behave differently, we averaged simulation results from both modes to generate un-polarized spectra (Figure 6c blue and green curves). Un-polarized backward scattering spectra of NHAs were simulated for both ECP-ox and ECP-neu states of the polymer coating (Figure 6d,e). It is clear from direct comparison, a general fair match in the main peak locations is observed for both states with excessive reflection at longer wavelength as discussed above. In addition, the simulated spectra showed multiple secondary modes underlying a single peak not detected in experimental spectra due probably to preferential source polarization (as discussed later), limited spectral resolution, and NHA fabrication imperfections.

Despite these complications, the calculated spectra are broadly in agreement with our experimental observation of significant differences in the modulation behavior of forward vs. backward scattering of polymer infused NHAs under variable electrochemical potential. Both the relative ratio between the two peaks (as a measurement of attenuation) in the forward scattering, and the peak position (as a measurement of refractive index induced plasmonic peak shifting) in the backward scattering, are replicated and suggest that plasmon modes excited in the backscattering setup are more sensitive towards changes in the refractive index compared to those excited in the forward scattering (Figure 6f).

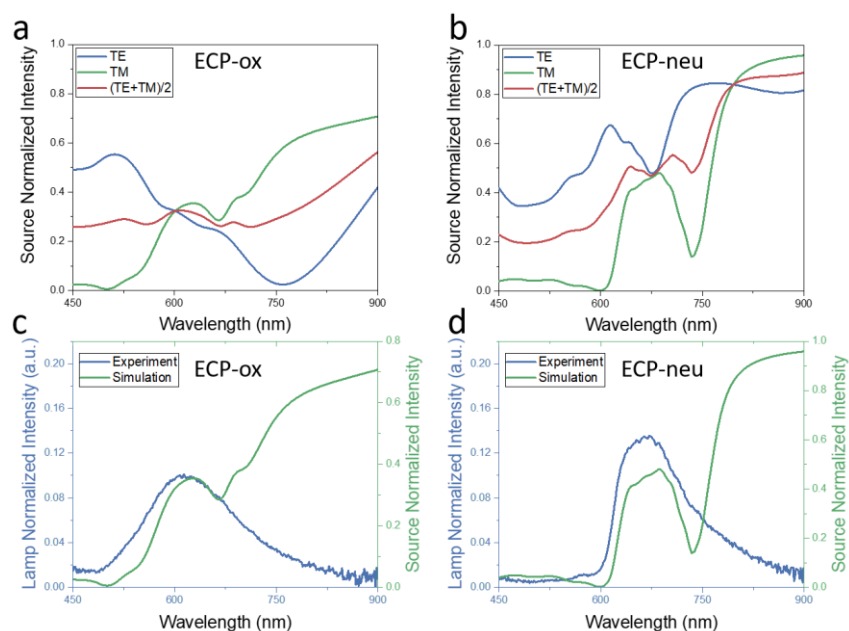


**Figure 7.** Decomposition of FDTD simulated unpolarized back scattering spectra of p250s array into TE and TM polarized components for ECP oxidized (a) and neutral (b) states. Measured backward scattering spectra (blue) of p250s array compared with FDTD results of pure TM polarized light (green) for ECP oxidized (c) and neutral (d) states.

In addition, the simulation suggests the plasmonic resonances excited by TE and TM polarization modes behave very differently from each other (Figure 7a, b). Changes in refractive index also prompted much larger response when the two modes are individually considered. It is possible that at highly oblique angle of illumination, slight changes in the permittivity of the infused polymer can cause totally different plasmonic modes to be excited in the NHA. Interestingly, further comparison of the simulated spectrum with experimental results indicated sources with pure TM polarization produced a better fit

than unpolarized sources, suggesting preferential TM polarized illumination. This is expected, as in our reflected darkfield setup, the illumination light column goes through a reflector lens assembly that partially polarizes the illuminating light. However, quantitative ratio of this polarization is unknown, so simulations using unpolarized sources are still presented here for demonstration of the universality.

A natural supplement to this work would be to investigate the optical properties of NHAs under transmission darkfield setup, in which light is coming from beneath the substrate at a highly oblique angle and the spectrum is collected by objectives lens above the substrate (Figure S5a). Due to limitations in our hyperspectral system setup, we cannot conduct such an experiment. However, we did simulate the response of p250s array under such conditions (Figure S5). The results suggest the transmission intensities are very low ( $< 1\%$ ), and there exist a cut-off frequency where almost no light is transmitted. ECP modulations do seem to produce large spectral variations and have some interesting characteristics of interest for future research (see Figure S5 and relevant discussion in SI).

## Conclusions

In summary, we have observed dramatic differences in the forward and backward scattering properties of polymer-infused plasmonic NHAs under variable matrix permittivity modulated by electrochemical potential. The modulation of backward scattering is significantly different compared to scattering in the forward direction. Although for forward scattering, the effect of ECP modulation is mostly dominated by attenuation of plasmonic peaks, the backward scattering of NHAs show large peak shifts due to the changes in plasmon resonance conditions. These asymmetrical optical response of polymer-metal NHA structures can be useful for various prospective applications, such as logic operations in photonic circuits.<sup>41, 42, 43</sup> The polarization and angle dependent backscattering response might find use in configuring plasmonic-based color filter with novel illumination geometries.<sup>44</sup> Finally, the extreme refractive index sensitivity of polymer-metal NHAs in the backward scattering setup could be further extended to SPR-type molecular sensors<sup>45, 46, 47</sup> with improved performance in the

detection of subtle refractive index modulation caused by absorption events.<sup>48, 49, 50, 51, 52, 53</sup>

### **Conflict of Interest**

The authors declare no conflict of interest.

### **Acknowledgments**

The authors thank the U.S. Department of Energy, Office of Basic Energy Sciences, Division of Materials Sciences and Engineering Award # DE-FG02-09ER46604 (fabrication of NHAs, FDTD simulations), Air Force Office of Scientific Research Award FA9550-14-1-0037 (optical characterizations), and the National Science Foundation, CHE-1506046 (ECP synthesis, electrochemistry) for funding. The NHA fabrication was performed in part at the Georgia Tech Institute for Electronics and Nanotechnology, a member of the National Nanotechnology Coordinated Infrastructure, which is supported by the National Science Foundation (Grant ECCS-1542174).

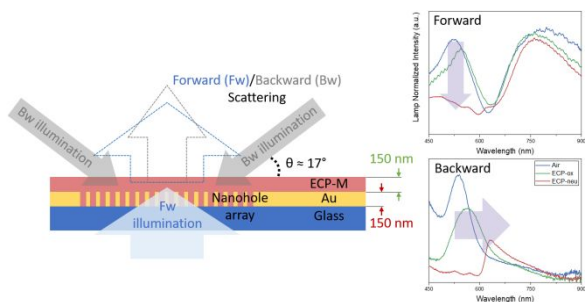
## References

- [1] T. W. Ebbesen, H. J. Lezec, H. Ghaemi, T. Thio and P. Wolff, Extraordinary optical transmission through sub-wavelength hole arrays, *Nature*, 1998, **391**, 667-669.
- [2] F. J. Garcia-Vidal, L. Martin-Moreno, T. Ebbesen and L. Kuipers, Light passing through subwavelength apertures, *Rev. Mod. Phys.*, 2010, **82**, 729-787.
- [3] W. L. Barnes, A. Dereux and T. W. Ebbesen, Surface plasmon subwavelength optics, *Nature*, 2003, **424**, 824-830.
- [4] C. Genet and T. W. Ebbesen, Light in tiny holes, *Nature*, 2007, **445**, 39-46.
- [5] L. Shao, X. Zhuo and J. Wang, Advanced Plasmonic Materials for Dynamic Color Display, *Adv. Mater.*, 2018, **30**, 1704338.
- [6] D. Y. Lei, J. Li, A. I. Fernández-Domínguez, H. C. Ong and S. A. Maier, Geometry Dependence of Surface Plasmon Polariton Lifetimes in Nanohole Arrays, *ACS Nano*, 2010, **4**, 432-438.
- [7] L. Martin-Moreno, F. Garcia-Vidal, H. Lezec, K. Pellerin, T. Thio, J. Pendry and T. Ebbesen, Theory of extraordinary optical transmission through subwavelength hole arrays, *Phys. Rev. Lett.*, 2001, **86**, 1114.
- [8] Z. Tang, R. Peng, Z. Wang, X. Wu, Y. Bao, Q. Wang, Z. Zhang, W. Sun and M. Wang, Coupling of surface plasmons in nanostructured metal/dielectric multilayers with subwavelength hole arrays, *Phys. Rev. B*, 2007, **76**, 195405.
- [9] F. Gao, D. Li, R.-W. Peng, Q. Hu, K. Wei, Q. Wang, Y. Zhu and M. Wang, Tunable interference of light behind subwavelength apertures, *Appl. Phys. Lett.*, 2009, **95**, 011104.
- [10] S. Yokogawa, S. P. Burgos and H. A. Atwater, Plasmonic Color Filters for CMOS Image Sensor Applications, *Nano Lett.*, 2012, **12**, 4349-4354.
- [11] Q. Chen and D. R. Cumming, High transmission and low color cross-talk plasmonic color filters using triangular-lattice hole arrays in aluminum films, *Opt. Express*, 2010, **18**, 14056-14062.
- [12] B. Zeng, Y. Gao and F. J. Bartoli, Ultrathin nanostructured metals for highly transmissive plasmonic subtractive color filters, *Sci. Rep.*, 2013, **3**, 2840.
- [13] T. Xu, Y.-K. Wu, X. Luo and L. J. Guo, Plasmonic nanoresonators for high-resolution colour filtering and spectral imaging, *Nat. Commun.*, 2010, **1**, 59.
- [14] F. Z. Shu, F. F. Yu, R. W. Peng, Y. Y. Zhu, B. Xiong, R. H. Fan, Z. H. Wang, Y. Liu and M. Wang, Dynamic Plasmonic Color Generation Based on Phase Transition of Vanadium Dioxide, *Adv. Opt. Mater.*, 2018, **6**, 1700939.
- [15] Y. Lee, M.-K. Park, S. Kim, J. H. Shin, C. Moon, J. Y. Hwang, J.-C. Choi, H. Park, H.-R. Kim and J. E. Jang, Electrical Broad Tuning of Plasmonic Color Filter Employing an Asymmetric-Lattice Nanohole Array of Metasurface Controlled by Polarization Rotator, *ACS Photonics*, 2017, **4**, 1954-1966.
- [16] T. Xu, E. C. Walter, A. Agrawal, C. Bohn, J. Velmurugan, W. Zhu, H. J. Lezec and A. A. Talin, High-contrast and fast electrochromic switching enabled by plasmonics, *Nat. Commun.*, 2016, **7**, 10479.
- [17] M. Atighilorestani, D. P. dos Santos, R. F. V. V. Jaimes, M. M. Rahman, M. L. A. Temperini and A. G. Brolo, Electrochemical Control of Light Transmission through Nanohole Electrode Arrays, *ACS Photonics*, 2016, **3**, 2375-2382.
- [18] K. Xiong, G. Emilsson, A. Maziz, X. Yang, L. Shao, E. W. Jager and A. B. Dahlin, Plasmonic Metasurfaces with Conjugated Polymers for Flexible Electronic Paper in Color, *Adv. Mater.*, 2016, **28**, 9956-9960.
- [19] K. Xiong, D. Tordera, G. Emilsson, O. Olsson, U. Linderhed, M. P. Jonsson and A. B. Dahlin, Switchable Plasmonic Metasurfaces with High Chromaticity Containing Only Abundant Metals, *Nano Lett.*, 2017, **17**, 7033-7039.
- [20] Z. Li, A. W. Clark and J. M. Cooper, Dual Color Plasmonic Pixels Create a Polarization Controlled Nano Color Palette, *ACS Nano*, 2016, **10**, 492-498.
- [21] Z. Zhou, Y. Yu, N. Sun, H. Möhwald, P. Gu, L. Wang, W. Zhang, T. A. F. König, A. Fery and G. Zhang, Broad-Range Electrically Tunable Plasmonic Resonances of a Multilayer Coaxial Nanohole Array with an Electroactive Polymer Wrapper, *ACS Appl. Mater. Interfaces*, 2017, **9**, 35244-35252.
- [22] S. Balakrishnan, M. Najiminaini, M. R. Singh and J. J. Carson, A study of angle dependent surface plasmon polaritons in nano-hole array structures, *J. Appl. Phys.*, 2016, **120**, 034302.
- [23] A. Baba, J. Lübber, K. Tamada and W. Knoll, Optical Properties of Ultrathin Poly(3,4-ethylenedioxythiophene) Films at Several Doping Levels Studied by In Situ Electrochemical Surface Plasmon Resonance Spectroscopy, *Langmuir*, 2003, **19**, 9058-9064.

- [24] J. F. Ponder, S. L. Pittelli and J. R. Reynolds, Heteroatom Role in Polymeric Dioxyselenophene-Dioxythiophene Systems for Color and Redox Control, *ACS Macro Letters*, 2016, **5**, 714-717.
- [25] N. B. Teran and J. R. Reynolds, Discrete Donor–Acceptor Conjugated Systems in Neutral and Oxidized States: Implications toward Molecular Design for High Contrast Electrochromics, *Chem. Mater.*, 2017, **29**, 1290-1301.
- [26] J. F. Ponder, A. M. Österholm and J. R. Reynolds, Conjugated Polyelectrolytes as Water Processable Precursors to Aqueous Compatible Redox Active Polymers for Diverse Applications: Electrochromism, Charge Storage, and Biocompatible Organic Electronics, *Chem. Mater.*, 2017, **29**, 4385-4392.
- [27] T. A. F. König, P. A. Ledin, J. Kerszulis, M. A. Mahmoud, M. A. El-Sayed, J. R. Reynolds and V. V. Tsukruk, Electrically Tunable Plasmonic Behavior of Nanocube–Polymer Nanomaterials Induced by a Redox-Active Electrochromic Polymer, *ACS Nano*, 2014, **8**, 6182-6192.
- [28] H. J. Hagemann, W. Gudat and C. Kunz, Optical constants from the far infrared to the x-ray region: Mg, Al, Cu, Ag, Au, Bi, C, and Al<sub>2</sub>O<sub>3</sub>, *J. Opt. Soc. Am.*, 1975, **65**, 742-744.
- [29] W. M. Haynes, *CRC handbook of chemistry and physics*, CRC press, Boca Raton, 2014.
- [30] P. A. Ledin, J.-W. Jeon, J. A. Geldmeier, J. F. Ponder, M. A. Mahmoud, M. El-Sayed, J. R. Reynolds and V. V. Tsukruk, Design of Hybrid Electrochromic Materials with Large Electrical Modulation of Plasmonic Resonances, *ACS Appl. Mater. Interfaces*, 2016, **8**, 13064-13075.
- [31] J. J. Mock, D. R. Smith and S. Schultz, Local Refractive Index Dependence of Plasmon Resonance Spectra from Individual Nanoparticles, *Nano Lett.*, 2003, **3**, 485-491.
- [32] J.-W. Jeon, P. A. Ledin, J. A. Geldmeier, J. F. Ponder, M. A. Mahmoud, M. El-Sayed, J. R. Reynolds and V. V. Tsukruk, Electrically Controlled Plasmonic Behavior of Gold Nanocube@Polyaniline Nanostructures: Transparent Plasmonic Aggregates, *Chem. Mater.*, 2016, **28**, 2868-2881.
- [33] J.-W. Jeon, J. Zhou, J. A. Geldmeier, J. F. Ponder Jr, M. A. Mahmoud, M. El-Sayed, J. R. Reynolds and V. V. Tsukruk, Dual-Responsive Reversible Plasmonic Behavior of Core–Shell Nanostructures with pH-Sensitive and Electroactive Polymer Shells, *Chem. Mater.*, 2016, **28**, 7551-7563.
- [34] J. Zhou, J.-W. Jeon, J. F. Ponder, J. A. Geldmeier, M. A. Mahmoud, M. El-Sayed, J. R. Reynolds and V. V. Tsukruk, Electrochromic tuning of transparent gold nanorods with poly [(3, 4-propylenedioxy) pyrrole] shells in the near-infrared region, *J. Mater. Chem. C*, 2017, **5**, 12571-12584.
- [35] N. Jiang, X. Zhuo and J. Wang, Active Plasmonics: Principles, Structures, and Applications, *Chem. Rev.*, 2018, **118**, 3054-3099.
- [36] S. J. Tan, L. Zhang, D. Zhu, X. M. Goh, Y. M. Wang, K. Kumar, C.-W. Qiu and J. K. W. Yang, Plasmonic Color Palettes for Photorealistic Printing with Aluminum Nanostructures, *Nano Lett.*, 2014, **14**, 4023-4029.
- [37] A. S. Roberts, A. Pors, O. Albrektsen and S. I. Bozhevolnyi, Subwavelength Plasmonic Color Printing Protected for Ambient Use, *Nano Lett.*, 2014, **14**, 783-787.
- [38] J. Olson, A. Manjavacas, L. Liu, W.-S. Chang, B. Foerster, N. S. King, M. W. Knight, P. Nordlander, N. J. Halas and S. Link, Vivid, full-color aluminum plasmonic pixels, *Proc. Natl. Acad. Sci. U.S.A.*, 2014, **111**, 14348-14353.
- [39] R. Gordon, M. Hughes, B. Leathem, K. L. Kavanagh and A. G. Brolo, Basis and Lattice Polarization Mechanisms for Light Transmission through Nanohole Arrays in a Metal Film, *Nano Lett.*, 2005, **5**, 1243-1246.
- [40] J. A. Geldmeier, M. A. Mahmoud, J.-W. Jeon, M. El-Sayed and V. V. Tsukruk, The effect of plasmon resonance coupling in P3HT-coated silver nanodisk monolayers on their optical sensitivity, *J. Mater. Chem. C*, 2016, **4**, 9813-9822.
- [41] M. Cohen, Z. Zalevsky and R. Shavit, Towards integrated nanoplasmonic logic circuitry, *Nanoscale*, 2013, **5**, 5442-5449.
- [42] Y. Fu, X. Hu, C. Lu, S. Yue, H. Yang and Q. Gong, All-optical logic gates based on nanoscale plasmonic slot waveguides, *Nano Lett.*, 2012, **12**, 5784-5790.
- [43] W.-S. Chang, B. A. Willingham, L. S. Slaughter, B. P. Khanal, L. Vigderman, E. R. Zubarev and S. Link, Low absorption losses of strongly coupled surface plasmons in nanoparticle assemblies, *Proc. Natl. Acad. Sci. U.S.A.*, 2011, **108**, 19879-19884.
- [44] Y. S. Do, J. H. Park, B. Y. Hwang, S. M. Lee, B. K. Ju and K. C. Choi, Plasmonic Color Filter and its Fabrication for Large-Area Applications, *Adv. Opt. Mater.*, 2013, **1**, 133-138.
- [45] F. Eftekhari, C. Escobedo, J. Ferreira, X. Duan, E. M. Girotto, A. G. Brolo, R. Gordon and D. Sinton, Nanoholes as nanochannels: flow-through plasmonic sensing, *Anal. Chem.*, 2009, **81**, 4308-4311.

- [46] A. G. Brolo, R. Gordon, B. Leathem and K. L. Kavanagh, Surface plasmon sensor based on the enhanced light transmission through arrays of nanoholes in gold films, *Langmuir*, 2004, **20**, 4813-4815.
- [47] H. Im, H. Shao, Y. I. Park, V. M. Peterson, C. M. Castro, R. Weissleder and H. Lee, Label-free detection and molecular profiling of exosomes with a nano-plasmonic sensor, *Nat. Biotechnol.*, 2014, **32**, 490-495.
- [48] S. Zhang, R. Geryak, J. Geldmeier, S. Kim and V. V. Tsukruk, Synthesis, Assembly, and Applications of Hybrid Nanostructures for Biosensing, *Chem. Rev.*, 2017, **117**, 12942-13038.
- [49] M. Couture, K. K. Ray, H.-P. Poirier-Richard, A. Crofton and J.-F. Masson, 96-Well Plasmonic Sensing with Nanohole Arrays, *ACS Sensors*, 2016, **1**, 287-294.
- [50] J. A. Jackman, A. R. Ferhan and N.-J. Cho, Nanoplasmonic sensors for biointerfacial science, *Chem. Soc. Rev.*, 2017, **46**, 3615-3660.
- [51] V. Canalejas-Tejero, S. Herranz, A. Bellingham, M. C. Moreno-Bondi and C. A. Barrios, Passivated Aluminum Nanohole Arrays for Label-Free Biosensing Applications, *ACS Appl. Mater. Interfaces*, 2014, **6**, 1005-1010.
- [52] S. Barbosa, A. Agrawal, L. Rodríguez-Lorenzo, I. Pastoriza-Santos, R. A. Alvarez-Puebla, A. Kornowski, H. Weller and L. M. Liz-Marzán, Tuning Size and Sensing Properties in Colloidal Gold Nanostars, *Langmuir*, 2010, **26**, 14943-14950.
- [53] L. Polavarapu and L. M. Liz-Marzán, Towards low-cost flexible substrates for nanoplasmonic sensing, *Phys. Chem. Chem. Phys.*, 2013, **15**, 5288-5300.

TOC:



**Electrochromic polymer infused plasmonic nanohole array show heterogeneous forward and backward optical scattering response upon polymer electrical permittivity modulation.**